View metadata, citation and similar papers at core.ac.uk

brought to you by CORE

provided by Carolina Digital Repository

THE JOURNAL OF BIOLOGICAL CHEMISTRY
Vol. 277, No. 35, Issue of August 30, pp. 31551–31562, 2002
© 2002 by The American Society for Biochemistry and Molecular Biology, Inc.
Printed in U.S.A.

Structure-Function Relationships of the RNA-dependent RNA Polymerase from Poliovirus (3Dpol)

A SURFACE OF THE PRIMARY OLIGOMERIZATION DOMAIN FUNCTIONS IN CAPSID PRECURSOR PROCESSING AND VPg URIDYLYLATION*

Received for publication, May 6, 2002, and in revised form, June 13, 2002
Published, JBC Papers in Press, June 19, 2002, DOI 10.1074/jbc.M204408200

Harsh B. Pathak‡§, Saikat Kumar B. Ghosh‡§, Allan W. Roberts¶, Suresh D. Sharma‡, Joshua D. Yoder‡‖, Jamie J. Arnold‡, David W. Gohara‡‖, David J. Barton¶, Aniko V. Paul, and Craig E. Cameron‡ ‡‡**

*From the ‡Department of Biochemistry and Molecular Biology, Pennsylvania State University, University Park, Pennsylvania 16802, the ¶Department of Microbiology, University of Colorado Health Sciences Center, Denver, Colorado 80262, and the **Department of Molecular Genetics and Microbiology, State University of New York, Stony Brook, New York 11794*

The primary oligomerization domain of poliovirus polymerase, 3Dpol, is stabilized by the interaction of the back of the thumb subdomain of one molecule with the back of the palm subdomain of a second molecule, thus permitting the head-to-tail assembly of 3Dpol monomers into long fibers. The interaction of Arg-455 and Arg-456 of the thumb with Asp-339, Ser-341, and Asp-349 of the palm is key to the stability of this interface. We show that mutations predicted to completely disrupt this interface do not produce equivalent growth phenotypes. Virus encoding a polymerase with changes of both residues of the thumb to alanine is not viable; however, virus encoding a polymerase with changes of all three residues of the palm to alanine is viable. Biochemical analysis of 3Dpol derivatives containing the thumb or palm substitutions revealed that these derivatives are both incapable of forming long fibers, suggesting that polymerase fibers are not essential for virus viability. The RNA binding activity, polymerase activity, and thermal stability of these derivatives were equivalent to that of the wild-type enzyme. The two significant differences observed for the thumb mutant were a modest reduction in the ability of the altered 3CD proteinase to process the VP0/VP3 capsid precursor and a substantial reduction in the ability of the altered 3Dpol to catalyze oriI-templated uridylylation of VPg. The defect to uridylylation was a result of the inability of 3CD to stimulate this reaction. Because 3C alone can substitute for 3CD in this reaction, we conclude that the lethal replication phenotype associated with the thumb mutant is caused, in part, by the disruption of an interaction between the back of the thumb of 3Dpol and some undefined domain of 3C. We speculate that this interaction may also be critical for assembly of other complexes required for poliovirus genome replication.

The RNA-dependent RNA polymerase (RdRP)[1] is the key component of the replication machinery of RNA viruses. The RdRP from poliovirus (3Dpol) serves as a paradigm for this class of nucleic acid polymerases. The crystal structure for 3Dpol (1) revealed that this polymerase has the typical topology observed for other nucleic acid polymerases and can be compared with a cupped, right hand with fingers, palm, and thumb subdomains (Fig. 1*A*). A unique feature of this polymerase, however, is the presence of two extensive regions of polymerase-polymerase interactions, referred to as interface I and interface II (1). Polymerase molecules interact in a "head-to-tail" fashion to form long, extended fibers via interface I, and these fibers interact with each other via interface II. Interface I is formed by an interaction between the back of the thumb of one polymerase molecule and the back of the palm of a second polymerase molecule (Fig. 1*B*). A few of the critical interactions required for integrity of interface I are shown in Fig. 1*C*. Specifically, Arg-455 and Arg-456 of the thumb subdomain of one polymerase molecule interact with Asp-339, Ser-341, and Asp-349 of the palm subdomain of the second polymerase molecule (Fig. 1*C*).

A variety of biochemical studies have provided additional evidence for oligomerization of 3Dpol. For example, filter-binding studies, performed in a manner that separates oligomers greater than 100 molecules from smaller assemblies, demonstrate a concentration-dependent increase in formation of large 3Dpol oligomers at low pH values (2–4). In addition, glutaraldehyde cross-linking studies provide evidence for the existence of 3Dpol multimers (2). Finally, 3Dpol exhibits cooperativity with respect to polymerase activity (2). However, it should be noted that the observed cooperative nature of polymerase activity is not observed in all cases (5) and may either be substrate-dependent (5) or a reflection of the absence or presence of certain divalent cations, in particular Zn^{2+} ions (4). It is worth noting that the ability of 3Dpol molecules to interact has also been demonstrated by using the yeast two-hybrid system (6, 7).

Clustered charged-to-alanine mutagenesis of 3Dpol identified residues Arg-455 and Arg-456 as residues essential for

* This work was supported in part by the National Institutes of Health through Howard Temin Award CA75118 (to C. E. C.) from NCI and Grants AI45818 (to C. E. C.) and AI42189 (to D. J. B.) from NIAID. The costs of publication of this article were defrayed in part by the payment of page charges. This article must therefore be hereby marked "*advertisement*" in accordance with 18 U.S.C. Section 1734 solely to indicate this fact.

§ These authors contributed equally to this work.
‖ Current address: Dept. of Biological Chemistry and Molecular Pharmacology, Harvard Medical School, Boston, MA 02115.
‡‡ To whom correspondence should be addressed. Tel.: 814-863-8705; Fax: 814-865-7927; E-mail: cec9@psu.edu.

[1] The abbreviations used are: RdRP, RNA-dependent RNA polymerase; DMEM, Dulbecco's modified Eagle's medium; Tricine, *N*-[2-hydroxy-1,1-bis(hydroxymethyl)ethyl]glycine; MOPS, 4-morpholinepropanesulfonic acid; MES, 4-morpholineethanesulfonic acid; oligo, oligonucleotide; sym/sub, symmetrical substrate; PEI, polyethyleneimine; PBS, phosphate-buffered saline; nt, nucleotide(s); GdnHCl, guanidine HCl.

TABLE I
Oligonucleotides used in this study
Restriction sites are shown in bold; codons containing nucleotide changes are italicized.

No.	Name	Sequence
1	pMo-R455,456A-f	5′-TAC TCA ACA TTG TAC *GCT GCA* TGG CTT GAC TCA TTT TAG-3′
2	pMo-R455,456A-r	5′-CTA AAA TGA GTC AAG CCA *TGC AGC* GTA CAA TGT TGA GTA-3′
3	pMo-BglII-f	5′-GAA GTG G**AG ATC T**TG GAT GCC AAA GCG-3′
4	pMo-EcoRI-r	5′-GAA TTA AAT CAT CGA T**GA ATT C**GG GCC C-3′
5	N-term Ub	5′-ACG CTG TCT GAT TAC AAC-3′
6	pET-3D-r	5′-TTG GCT TGA CTC ATT TTA GTA AGG ATC CGA ATT CCG C-3′
7	NheI-f	5′-GTT GAC GCT AGT CT**G CTA GC**C CAA TCA GGA AAA-3′
8	R455,456A-EcoRI-r	5′-GCG **GAA TTC** TTA CTA AAA TGA GTC AAG CCA *TGC AGC* GTA CAA TGT TGA GTA-3′
9	R455,456S-EcoRI-r	5′-GCG **GAA TTC** TTA CTA AAA TGA GTC AAG CCA *GGA AGA* GTA CAA TGT TGA GTA-3′
10	R455,456D-EcoRI-r	5′-GCG **GAA TTC** TTA CTA AAA TGA GTC AAG CCA *GTC GTC* GTA CAA TGT TGA GTA-3′
11	3D-KpnI-f	5′-GGC TGC TCA **GGT ACC** TCA ATT TTT AAC-3′
12	3D-D339A,S341A-r	5′-CCT GAT TGG **GCT AGC** AG*A GCA* GC*A GCA* ACT TCA TGG-3′
13	3D-NheI-D349A-f	5′-GCT CT**G CTA GC**C CAA TCA GGA AAA *GCT* TAT GGA CTA AC-3′
14	3D-NcoI-EcoRI-r	5′-CGG AGC TC**G AAT TCC CAT GG**T TAC TAA AAT G-3′
15	3C-SacII-f	5′-GCG GAA TTC CT**C CGC GG**T GGA GGA CCA GGG TTC GAT T-3′
16	3D-AflII-r	5′-AAA GTC TGT **CTT AAG** CCT GGG ATC G-3′
17[a]	3CD-H40G-f	5′-GCT ATT TTA CCA ACC *GGT* **GCT *AGC*** CCT GGT GAA AGC ATT-3′
18[a]	3CD-H40G-r	5′-AAT GCT TTC ACC AGG ***GCT* AGC** *ACC* GGT TGG TAA AAT AGC-3′
19	3C-Chis-BamHI-r	5′-GCG GGT ACC **GGA TCC** TTG ACT CTG AGT GAA GTA-3′
20	3C-C147G-f	5′-CCA ACC AGA GCA GGA CAG *GGT* GGT GGA GTC ATC ACA-3′
21	3C-C147G-r	5′-TGT GAT GAC TCC ACC *ACC* CTG TCC TGC TCT GGT TGG-3′
22[b]	BamHI-T761CRE-f	5′-CG**G GAT CC**T AAT ACG ACT CAC TAT AGG GTA TTA ACA ACT ACA TAC A-3′
23	61CRE-EcoRI-r	5′-G**GA ATT CGT ATA C**TA GCA AAC ATA CTG G-3′

[a] An *Nhe*I site was introduced via a silent mutation.
[b] The T7 promoter is underlined.

virus viability (8). Given the role of these residues in the stability of interface I (Fig. 1*C*) (1), these data provided the first evidence that oligomerization of 3Dpol might play a significant role in some step of the virus multiplication cycle. Subsequent studies of additional 3Dpol derivatives with modifications of residues involved in forming interface I provided additional support for the importance of this interface for 3Dpol function and virus viability (4). However, this study also presented an interesting paradox. Mutation of the residue that interacts with Arg-455, Asp-349, does not produce a lethal phenotype (4).

In this study, we test the hypothesis that the lethal phenotype associated with mutations on the back of the thumb of 3Dpol arises from a requirement for this subdomain that is independent of oligomerization. We find that 1) oligomerization via interface I may not be essential for virus multiplication and 2) the back of the thumb of 3Dpol may interact with host and viral factors to modulate capsid protein processing and initiation of protein-primed RNA synthesis, respectively. The implications of heteromeric interactions between 3Dpol and another viral factor on the mechanism for negative-strand RNA synthesis will be discussed.

EXPERIMENTAL PROCEDURES

Materials—DNA oligonucleotides were from Invitrogen and Integrated DNA Technologies, Inc.; T4 polynucleotide kinase, Deep Vent DNA polymerase, and restriction enzymes were from New England Biolabs, Inc.; shrimp alkaline phosphatase was from United States Biochemical Corp.; T4 DNA ligase and NZCYM were from Invitrogen; QIAEX was from Qiagen; Sephadex G-25 and RNase A were from Sigma; phosphocellulose (P-11) and DE-81 filter paper were from Whatman; all nucleotides (ultrapure solutions) and Q-Sepharose fast flow were from Amersham Biosciences; RNA oligonucleotides were from Dharmacon Research, Inc. (Boulder, CO); [α-^{32}P]UTP (6000 Ci/mmol) was from PerkinElmer Life Sciences; [γ-^{32}P]ATP (>7000 Ci/mmol) was from ICN; synthetic VPg peptide was from Alpha Diagnostic International (San Antonio, TX); all other reagents were available through Fisher or VWR.

Construction of Expression Plasmids for 3CD and 3C—Oligos 15 and 16 (Table I lists all oligonucleotides used in this study) were used to amplify the region encoding 3CD by using PCR and the viral cDNA (pMoRA, also known as pXpA-rib$^+$polyAlong (Ref. 9)) as template. The 3CD-coding region was cloned into pET26Ub-3D plasmid (10) by using the *Sac*II and *Afl*II sites to give pET26Ub-3CD. To inactivate the protease activity of 3CD, histidine 40 was changed to a glycine by using overlap-extension PCR with oligos 15–18 and pET26Ub-3CD plasmid as template. The product was cloned into pET26Ub-3CD to yield pET26Ub-3CD-H40G.

Cloning of the 3C gene was achieved by using oligos 15 and 19–21 and the viral cDNA (pMoRA (Ref. 9)) as template in overlap-extension PCR. The region was cloned into pET26Ub-Chis plasmid by using the *Sac*II and *Bam*HI sites to yield pET26Ub-3C-C147G-Chis. "C147G" designates mutation of cysteine 147 to a glycine to inactivate protease activity. The pET26Ub-Chis plasmid is designed to produce a C-terminal GSSG-His_6 tag for any protein cloned in by using the 3′ *Bam*HI site.

The pET26Ub expression plasmid for 3Dpol (pET26Ub-3D-BPKN) was previously described (10). DNA sequencing at the Pennsylvania State University Nucleic Acid Facility was used to verify the integrity of all clones.

Construction of Expression Plasmids for 3Dpol and 3CD Derivatives—The thumb mutations of Arg-455 and Arg-456 in 3Dpol were introduced by using reverse oligonucleotides encoding the Ala (oligo 8), Ser (oligo 9), or Asp (oligo 10) substitutions and the forward oligonucleotide (oligo 7). PCR products were cloned into pET26Ub-3D-BPKN plasmid (10) using the *Nhe*I and *Eco*RI sites. Palm mutations of Asp-339, Ser-341, and Asp-349 to alanine in 3Dpol were introduced by using overlap extension PCR using oligos 11–14. The PCR product was cloned into pET26Ub-3D-BPKN plasmid (10) using the *Kpn*I and *Eco*RI sites.

The thumb (R455A,R456A) and palm (D339A,S341A,D349A) mutations were introduced into 3CD by digesting the region containing the mutations in the pET26-Ub-3D-BPKN plasmid and ligating into the pET26Ub-3CD-H40G plasmid. The *Bst*BI and *Eco*RI sites were used to introduce the thumb mutations into 3CD; the *Bst*BI and *Mfe*I sites were used to introduce the palm mutations into 3CD. DNA sequencing confirmed the integrity of all clones.

Expression and Purification of 3Dpol, 3CD, and 3C Derivatives—All proteins expressed from the pET26Ub-based plasmids constructed above are N-terminally fused to yeast ubiquitin. Overexpression of protein in this system is performed in the BL21(DE3)pCG1 strain of *Escherichia coli*; this strain carries the pCG1 plasmid, which constitutively expresses a yeast ubiquitin protease that processes the ubiquitin fusion protein to produce the authentic N terminus (10). Expression, lysis, polyethyleneimine (PEI) precipitation, and ammonium sulfate precipitation for all 3Dpol and 3CD derivatives were performed as previously described (10). After suspension of the ammonium sulfate pellets in buffer A (50 mM Tris, pH 8.0, 20% glycerol, 1 mM dithiothre-

itol, 0.1% Nonidet P-40, and 60 μM $ZnCl_2$), the samples were dialyzed overnight against buffer A containing 10 mM NaCl. Spectra/Por dialysis tubing (Spectrum Laboratories Inc.) with a molecular mass cut-off of 12,000–14,000 Da was used. All of the steps of the purification were performed either on ice or at 4 °C. After dialysis, the conductivity of the protein was adjusted to 50 mM NaCl and the protein was loaded at 1 ml/min onto a phosphocellulose (P-11) column that was equilibrated with buffer A containing 50 mM NaCl. Approximately 1 ml of resin was used per 20 mg of total protein. Protein concentration was measured by using the Bio-Rad protein assay. The column was washed to baseline with buffer A containing 50 mM NaCl and protein was eluted by using a six-column volume, linear gradient from 50 to 350 mM NaCl in buffer A. Fractions (0.1 bed volume of the column) were collected and assayed for purity by SDS-PAGE. Conductivity of the pooled fractions was adjusted to 50 mM NaCl by using buffer A and the pooled fractions were loaded at 1 ml/min onto a Q-Sepharose column equilibrated with buffer A containing 50 mM NaCl. Again, 1 ml of resin was used per 20 mg of total protein. Washing was the same as for the P-11 column; protein was eluted using a six-column volume, linear gradient from 50 to 500 mM NaCl in buffer A. Fractions (0.1 bed volume of the column) were collected and assayed for purity by SDS-PAGE. Conductivity of the pooled fractions was adjusted to 50 mM NaCl using buffer A. This pool was loaded at 1 ml/min onto a 0.5-ml Q column equilibrated as described above. The column was washed to baseline using buffer B (50 mM HEPES, pH 7.5, 20% glycerol, 10 mM 2-mercaptoethanol, 0.1% Nonidet P-40, and 60 μM $ZnCl_2$) containing 50 mM NaCl. Protein was eluted from this Q column by using buffer B containing 500 mM NaCl. Fractions (0.5 ml) were collected until the concentration of the eluted protein fell below the desired value. Protein concentration was determined by using the following extinction coefficients: 0.071830 $\mu M^{-1}\cdot cm^{-1}$ (3Dpol) and 0.079510 $\mu M^{-1}\cdot cm^{-1}$ (3CD). These values were determined by using the protein parameters tool on the ExPASy site (us.expasy.org/tools/protparam.html). The absorbance values were measured at 280 nm in 6 M guanidine HCl (GdnHCl), pH 6.5. The conductivity of the individual fractions was measured; the fractions were aliquoted and stored at −80 °C.

3C was expressed essentially as described for 3Dpol and 3CD (10); however, a different lysis buffer was employed (50 mM HEPES, pH 7.5, 20% glycerol, 10 mM 2-mercaptoethanol, 5.6 μg/ml pepstatin A, 4 μg/ml leupeptin, 0.1 mM EDTA, and 500 mM NaCl). Phenylmethylsulfonyl fluoride and Nonidet P-40 were added after lysis to a final concentration of 1 mM and 0.1% (v/v), respectively. PEI was added to a final concentration of 0.25% (v/v); the lysate was stirred slowly at 4 °C for 30 min and then centrifuged in a Beckman Ti-60 rotor for 30 min at 30,000 rpm at 4 °C. The conductivity of the PEI supernatant was adjusted to 50 mM NaCl, and the supernatant was passed through a Q-Sepharose column followed in tandem by a P-11 column. Both columns were equilibrated with buffer C (50 mM HEPES, pH 7.5, 20% glycerol, 10 mM 2-mercaptoethanol, and 0.1% Nonidet P-40) containing 50 mM NaCl prior to loading. Approximately 1 ml of resin/80 mg of total protein was used for the Q column, and ~1 ml of resin/500 mg of total protein was used for the P-11 column. After all of the protein passed through the Q column, the P-11 column was detached and washed with 10 column volumes of buffer C containing 50 mM NaCl. 3C was eluted from the P-11 column by using buffer C containing 2 M NaCl. Fractions (1 ml) were eluted until the concentration of the eluted protein fell below the desired value. The high NaCl concentration was reduced from the fractions by dialysis against buffer C containing 250 mM NaCl using Spectra/Por dialysis tubing with a molecular mass cut-off of 6000–8000 Da. SDS-PAGE was used to assess the purity of the eluted fractions. Protein concentration was determined as described for 3Dpol and 3CD; the extinction coefficient used was 0.007680 $\mu M^{-1}\cdot cm^{-1}$. The conductivity of the individual fractions was measured; the fractions were aliquoted and stored at −80 °C.

Construction of Mutated Viral cDNA Clones and Mutated Replicons—Introduction of mutations into the thumb subdomain in the viral cDNA required overlap extension PCR by using oligos 1–4; the viral cDNA, pMoRA (9), was used as the template. The PCR product was digested with *Mfe*I and *Eco*RI and subcloned into the intermediate plasmid, pUC18-*Bgl*II-*Eco*RI-3CD (referred to as pUC-3CD in Ref. 11). From this subclone, the fragment between *Bgl*II and *Eco*RI was cloned into the viral cDNA (pMoRA (Ref. 9)) to yield the thumb mutant viral cDNA (pMoRA-R455A,R456A). For the introduction of mutations to the palm subdomain, PCR amplification from the expression vector containing the palm mutations (pET26Ub-3D-BPKN-D339A,S341A, D349A) was performed using oligos 5 and 6; the fragment between *Bst*BI and *Mfe*I was subcloned into the pUC18-*Bgl*II-*Eco*RI-3CD intermediate and from there to the viral cDNA using the *Bgl*II and *Eco*RI sites to yield the palm mutant viral cDNA (pMoRA-D339A,S341A, D349A). To introduce mutations into the replicon, the fragment between the *Bgl*II and *Apa*I sites from the mutated viral cDNAs was cloned into pRLucRA (also known as pRLuc31-rib$^+$polyAlong (Refs. 9 and 12)) to yield pRLucRA-R455A,R456A and pRLucRA-D339A,S341A,D349A. DNA sequencing was used to verify the integrity of all clones.

Infectious Center Assays—RNA transcripts were generated according to the instructions of the manufacturer for the T7-MEGAscript kit (Ambion, Inc.) after linearization with *Eco*RI. DNase treatment was used to remove the template; lithium chloride precipitation was used to remove unincorporated nucleotides. RNA concentration was calculated by measuring absorbance at 260 nm, assuming an A_{260} of 1 was equivalent to 40 μg/ml.

HeLa cells were propagated in DMEM/F-12 (Invitrogen) supplemented with 10% fetal bovine serum (Invitrogen), always keeping the cultures between 20 and 80% confluence. Subconfluent monolayers of HeLa cells were detached from the culture flasks by trypsin treatment, washed with 1× phosphate-buffered saline (PBS), and cell number adjusted to 3×10^6 cells/ml in PBS. Cell suspension (400 μl) was mixed with 10 μg of RNA (wild-type (pMoRA), thumb mutant (pMoRA-R455A,R456A), or palm mutant (pMoRA-D339A,S341A,D349A) viral transcripts) in a microcentrifuge tube, transferred to an electroporation cuvette (0.2-cm gap width; Bio-Rad) and subjected to an electric pulse at 500 microfarads and 130 V using a Gene Pulser system (Bio-Rad). Electroporated cells were diluted either 10- or 100-fold in PBS, and 100 μl of each dilution were plated on 2×10^5 HeLa cells (prepared 1 day in advance) in six-well dishes; 400 μl of DMEM/F-12 were added to each well. Undiluted electroporated cells (100 μl) were also plated using the same procedure. Cells were allowed to adsorb to the plate for 1 h at 37 °C, and then the medium/PBS was aspirated; the cells were covered with 3 ml of a mixture of 1× DMEM/F-12 plus 10% fetal bovine serum and 1% low melting point agarose (American Bioanalytical). Plates were then incubated at 37 °C for 3 days. The agarose overlay was removed by using a spatula. Wells were stained with crystal violet, and viral plaques were counted.

Subgenomic Replicon Assays—RNA transcripts were generated as described for the viral genomes from *Apa*I-linearized plasmids encoding the wild-type (pRLucRA (Refs. 9 and 12)), the thumb mutant (pRLucRA-R455A,R456A) or the palm mutant (pRLucRA-D339A,S341A, D349A) subgenomic replicons. HeLa cells were propagated as described for the infectious center assays. HeLa cells were transfected with subgenomic replicons (20 μg) by using electroporation. Electroporated cells were immediately transferred to prewarmed (37 °C) DMEM/F-12 as follows. The volume of the electroporated cells added was calculated by multiplying 33 μl by $n + 1$ (where n is the number of time points to be measured). The volume of DMEM/F-12 to which the electroporated cells were added was calculated by multiplying 500 μl by $n + 1$ (where n is the number of time points to be measured). After mixing the appropriate volume of electroporated cells with the appropriate volume of medium, 500-μl aliquots were prepared in microcentrifuge tubes for each time point to be measured. These aliquots were then incubated in a water bath at 37 °C without any agitation. At fixed time points, cells were pelleted by centrifugation at 14,000 × g for 2 min in an Eppendorf microcentrifuge. Lysis was performed by using 100 μl of 1× cell culture lysis reagent (Promega) and placed on ice for 2 min before removal of cellular debris and nuclei by centrifugation at 14,000 × g for 1 min. Lysates were left on ice at 4 °C until all time points were collected. Lysates were assayed for luciferase activity by mixing 10 μl of lysate with 10 μl of luciferase assay substrate (Promega) and quantifying light production by using a Lumat LB 9501 luminometer (Berthold).

HeLa S10 Translation-Replication Reactions (13)—HeLa cell S10 extract (S10) and HeLa cell translation initiation factors were prepared as previously described (14). HeLa S10 translation-replication reaction mixtures contained 50% by volume S10, 20% by volume initiation factors, 10% by volume 10× nucleotide reaction mix (10 mM ATP, 2.5 mM GTP, 2.5 mM UTP, 600 mM KCH_3CO_2, 300 mM creatine phosphate, 4 mg/ml creatine kinase, and 155 mM HEPES-KOH, pH 7.4), 2 mM GdnHCl, and viral mRNA at 50 μg/ml.

mRNA Translation (13)—Poliovirus mRNA translation was assayed by including [^{35}S]methionine (1.2 mCi/ml; Amersham Biosciences) in HeLa S10 translation-replication reaction mixtures. After 3 h of incubation at 34 °C, samples (4 μl) of the HeLa S10 translation-replication reaction mixtures containing [^{35}S]methionine were mixed with 100 μl of SDS-PAGE sample buffer (2% SDS (Sigma), 62.5 mM Tris-HCl, pH 6.8, 0.5% 2-mercaptoethanol, 0.1% bromphenol blue, 20% glycerol). The samples were heated at 100 °C for 5 min, and 25-μl portions of each sample were loaded onto a 0.75-mm-thick polyacrylamide gel (29:1,

acrylamide:bisacrylamide) consisting of a 4% stacking gel and a 9–18% gradient separating gel. The gels were fixed and dried; radiolabeled proteins were detected by phosphorimaging.

Poliovirus RNA Synthesis in Translation-Replication Reactions (13)—Poliovirus RNA synthesis was assayed using preinitiation RNA replication complexes formed in HeLa S10 translation-replication reaction mixtures as previously described (15). Briefly, viral RNAs (50 μg/ml) were incubated in S10 reaction mixtures containing 2 mM Gdn-HCl for 3 h at 34 °C. Preinitiation complexes were isolated from the reactions by centrifugation at 13,000 $\times$ *g* for 15 min at 4 °C. Pellets containing preinitiation complexes were then suspended in 50-μl labeling reaction mixtures containing [α-^{32}P]CTP and incubated at 37 °C for 60 min as previously described (method 4 in Ref. 15). Under these conditions, radiolabel was incorporated into nascent negative- and positive-strand RNA as it was synthesized. The reactions were centrifuged at 13,000 $\times$ *g* to pellet the viral RNA replication complexes. Radiolabeled viral RNA remained in the replication complexes.[2] The supernatant, containing unincorporated radiolabel, was discarded. The pellets were solubilized in SDS sample buffer. The products of the reaction were phenol/chloroform-extracted, ethanol-precipitated, and separated by electrophoresis in a 1% agarose MOPS formaldehyde gel. RNA in the gels was stained with ethidium bromide and visualized by UV light. ^{32}P-Labeled poliovirus RNA was detected and quantified by using a PhosphorImager (Bio-Rad).

VPg Uridylylation in Translation-Replication Reactions (13)—VPg uridylylation was assayed using preinitiation RNA replication complexes. Preinitiation RNA replication complexes were isolated from HeLa S10 translation-replication reaction material using the same procedure as described above for poliovirus RNA synthesis. The preinitiation RNA replication complexes were suspended in 50 μl of labeling reaction mixture containing [α-^{32}P]UTP rather than [α-^{32}P]CTP. The reaction mixtures were incubated for 60 min at 37 °C. Following incubation, the reaction mixtures were centrifuged at 13,000 $\times$ *g* to pellet the viral RNA replication complexes. Radiolabeled VPgpUpU and radiolabeled viral RNA remained in the replication complexes and were not released into the soluble portion of the reaction mixtures.[2] The supernatant, containing unincorporated radiolabel, was discarded. The pellets, containing radiolabeled viral RNA and uridylylated VPg, were solubilized in SDS sample buffer. The samples were fractionated by electrophoresis in a 10% polyacrylamide Tris-Tricine gel, and radiolabeled VPgpUpU was detected by phosphorimaging.

Trace Labeling of RNA (rU_{30})—The RNA oligonucleotide was end-labeled by using [γ-^{32}P]ATP and T4 polynucleotide kinase essentially as specified by the manufacturer. Reactions, typically 20 μl, contained 0.1 μM [γ-^{32}P]ATP, 10 μM RNA oligonucleotide (rU_{30}), 1$\times$ kinase buffer, and 0.4 units/μl T4 polynucleotide kinase. Reactions were incubated at 37 °C for 60 min and quenched by incubation at 65 °C for 5 min.

RNA Filter-binding Assays—Reaction mixtures, typically 50 μl, contained 10 nM trace-labeled rU_{30} and wild-type or mutant 3Dpol derivatives of varying concentrations in reaction buffer (25 mM MES-NaOH, pH 5.5, 60 mM NaCl, 5 mM $MgCl_2$, 0.1 mM $ZnSO_4$ 5 mM dithiothreitol, 0.25 mM ATP, 20% glycerol). 3Dpol was diluted immediately prior to use in enzyme dilution buffer (50 mM HEPES, pH 7.5, 10 mM 2-mercaptoethanol, 60 μM $ZnCl_2$ and 20% glycerol). Binding reactions were initiated by the addition of 5 μl of the diluted 3Dpol to the remaining components. Reactions were incubated on ice for 30 min. This assay employs three filters: polysulfone membrane, which traps any protein-nucleic acid complexes larger than 0.45 μm; a nitrocellulose membrane, which traps all other protein-nucleic acid complexes; and a nylon membrane, which binds all unbound nucleic acid. Membranes were presoaked in wash buffer (50 mM HEPES, pH 7.5, and 5 mM $MgCl_2$) and assembled, in order from top to bottom, polysulfone, nitrocellulose, and nylon, in a slot blotter (Invitrogen). After assembly, 20 μl of wash buffer were applied to each slot and filtered through all three membranes by applying a vacuum. After washing, 20 μl of each binding reaction were applied to each slot and filtered through the membranes. Membranes were air-dried and visualized by using a PhosphorImager (Amersham Biosciences) and quantified by using ImageQuant software (Amersham Biosciences).

Symmetrical Substrate (sym/sub)—Purification, 5′-^{32}P labeling, and annealing were performed as previously described (16).

3Dpol Elongation Assays—Reaction mixtures contained sym/sub and 3Dpol in reaction buffer (50 mM HEPES, pH 7.5, 10 mM 2-mercaptoethanol, 5 mM $MgCl_2$, 60 μM $ZnCl_2$, 500 μM NTP). Reactions were quenched by addition of EDTA to a final concentration of 50 mM. Specific concentrations of primer/template and 3Dpol, along with any deviations from the above, are indicated in the appropriate sections below. 3Dpol was diluted immediately prior to use in enzyme dilution buffer (50 mM HEPES, pH 7.5, 10 mM 2-mercaptoethanol, 60 μM $ZnCl_2$, and 20% glycerol). The volume of enzyme added to any reaction was always less than or equal to one-tenth of the total volume.

Product Analysis, Denaturing PAGE—Reaction products were analyzed by denaturing PAGE as previously described (16).

Active-site Titration—Reactions contained 20 μM sym/sub (10 μM duplex), 5 mM $MgCl_2$, 1 or 2.5 μM 3Dpol, and 500 μM ATP. Reactions were initiated by addition of 3Dpol and incubated at 30 °C; reactions were quenched at fixed time points by the addition of EDTA to a final concentration of 50 mM. The kinetic data best fit to a line. The *y* intercept represents the concentration of active 3Dpol.

Dissociation of 3Dpol-sym/sub Complexes—3Dpol (1 μM) was incubated with stoichiometrically labeled sym/sub (0.1 μM) for 90 s at 30 °C, at which point trap (100 μM unlabeled sym/sub) was added to the reaction. At fixed times after the addition of trap, ATP (500 μM) was added and the reaction was allowed to proceed for 30 s and then quenched by addition of EDTA (50 mM). Products were resolved by electrophoresis on a denaturing, highly cross-linked (1.7% bisacrylamide), 23% polyacrylamide gel as previously described (16). The kinetic data best fit to a single exponential.

Inactivation of 3Dpol—3Dpol (2 μM) was incubated at 30 °C in 1$\times$ reaction buffer (50 mM HEPES, pH 7.5, 10 mM 2-mercaptoethanol, 60 μM $ZnCl_2$, and 5 mM $MgCl_2$) and at the indicated times the reaction was initiated by addition of sym/sub (1 μM) and ATP (500 μM) and allowed to proceed for an additional 90 s at 30 °C, at which time the reaction was quenched by addition of EDTA (50 mM). The kinetic data best fit to a single exponential.

Rapid Chemical-quench-flow Experiments—Rapid mixing/quenching experiments were performed by using a model RQF-3 chemical-quench-flow apparatus (KinTek Corp., State College, PA). Experiments were performed at 30 °C by using a circulating water bath. 3Dpol-sym/sub complex in 50 mM HEPES, pH 7.5, 10 mM 2-mercaptoethanol, 60 μM $ZnCl_2$, and 5 mM $MgCl_2$ was rapidly mixed with the nucleotide substrate in 50 mM HEPES, pH 7.5, 10 mM 2-mercaptoethanol, 60 μM $ZnCl_2$, and 5 mM $MgCl_2$, and the reactions were quenched by addition of 0.5 M EDTA to a final concentration of 0.3 M.

Rate of Nucleotide Incorporation—3Dpol (2 μM) was incubated with 2 μM sym/sub (1 μM duplex) and rapidly mixed with 1000 μM ATP as described for the rapid chemical-quench-flow experiments. After mixing, reactant concentrations were reduced by 50%. Reactions were quenched at the fixed times by addition of 0.5 M EDTA to a final concentration of 0.3 M. The kinetic data best fit to a single exponential.

Poly(rU) Polymerase Activity Assays—Reactions contained 3Dpol (0.5 μM), 1.9 μM dT_{15} and 0.2 μM poly(rA)$_{400}$ primer/template in reaction buffer (50 mM HEPES, pH 7.5, 10 mM 2-mercaptoethanol, 5 mM $MgCl_2$, 60 μM $ZnCl_2$, 500 μM UTP, 0.4 μCi/μl [α-^{32}P]UTP). Reactions were initiated by addition of 3Dpol and were carried out in a total volume of 25 μl at 30 °C for 5 min; EDTA (50 mM final) was used to quench the reactions. The quenched reactions (5 μl) were spotted onto DE81 filter paper discs and dried completely. The discs were washed three times for 5, 10, and 5 min in 250 ml of 5% dibasic sodium phosphate and rinsed in absolute ethanol. Bound radioactivity was quantified by liquid scintillation counting in 5 ml of Ecoscint scintillation fluid (National Diagnostics).

Cloning and Transcription of 61-nt oriI—The region corresponding to the 61 nucleotides of oriI was amplified from an expression vector encoding the 2C gene.[3] A *Bam*HI site and a T7 promoter were included in the forward oligonucleotide (oligo 22) used for the PCR reaction; a *Bst*Z17I site was included immediately before the *Eco*RI site in the reverse oligonucleotide (oligo 23). This PCR product was cloned into a pUC18 vector using *Bam*HI and *Eco*RI sites; the cloning was confirmed by sequencing. The pUC18–61nt-oriI plasmid was linearized using the *Bst*Z17I site and a transcription reaction was performed according to the instructions of the manufacturer for the T7-MEGAshortscript kit (Ambion, Inc.). DNase treatment was used to remove the template; either the QuickClean Enzyme Removal Resin (CLONTECH) or Micropure-EZ centrifugal filters (Amicon Bioseparations, Millipore) was used to remove any protein from the RNA according to the instructions of the respective manufacturers. A Sephadex G-25 spun column was used to remove any unincorporated nucleotides. RNA concentration was calculated by measuring absorbance at 260 nm. The extinction coefficient was calculated for the 61-nt oriI plus three guanidine residues that are

[2] D. J. Barton, unpublished results.

[3] C. E. Cameron, unpublished results.

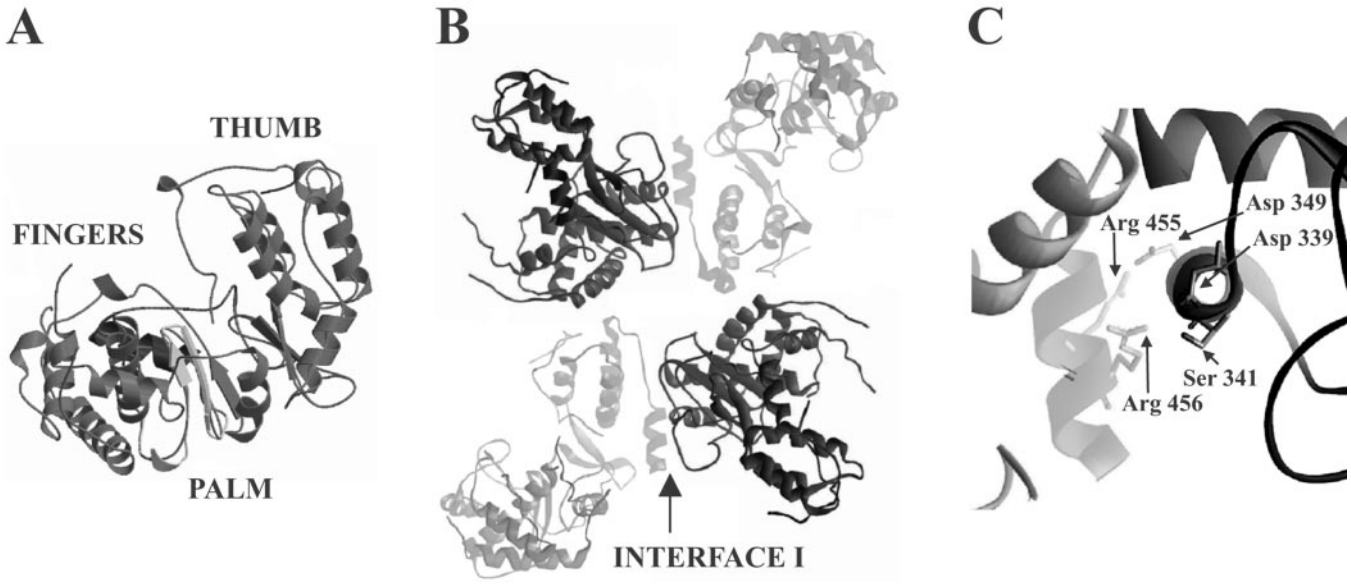

FIG. 1. **The primary oligomerization domain (interface I) of 3Dpol.** *A*, 3Dpol has the "right-hand" topology typical of all nucleic acid polymerases. *B*, 3Dpol molecules form head-to-tail fibers via interface I. Residues on the back of the thumb of one molecule interact with residues on the back of the palm of a second molecule. *C*, shown are a few of the critical interactions observed crystallographically for interface I. Arginines 455 and 456 of the thumb subdomain interact with aspartic acids 339 and 349 and serine 341 of the palm subdomain.

transcribed at the 5′ end of oriI (0.749400 $\mu M^{-1} \cdot cm^{-1}$) (17). The three G nucleotides were included to increase the efficiency of the transcription reaction; these three G nucleotides do not alter the fold of oriI in any way as predicted using the *mfold* RNA folding server available on the Zuker home page (bioinfo.math.rpi.edu/~zukerm/).

VPg Uridylylation Assays—Reaction mixtures contained 1 μM 3Dpol, 1 μM 3CD, 1 μM 61-nt oriI, and 50 μM VPg in reaction buffer (50 mM HEPES, pH 7.5, 10% glycerol, 5 mM magnesium acetate, 60 μM ZnCl, 10 mM 2-mercaptoethanol, 10 μM UTP, and 0.004 μM [α-^{32}P]UTP (6000 Ci/mmol)). All reactions were adjusted to a final NaCl concentration of 20 mM. 3Dpol and 3CD were diluted immediately prior to use. 5 μl of 4 μM 3Dpol and 5 μl of 4 μM 3CD were mixed together in one tube immediately prior to the initiation of the reactions and placed on ice; reactions were initiated by addition of 10 μl of reaction mix containing the remaining components to the 10-μl 3Dpol/3CD mix. Reaction mixtures were incubated at the indicated temperatures for 30 min and quenched with an equal volume (20 μl) of 100 mM EDTA in 90% formamide containing 0.05% bromphenol blue and xylene cyanol dyes. Quenched reactions (5 μl) were analyzed by using Tris-Tricine SDS-polyacrylamide gel electrophoresis. Gels contained 15% acrylamide and 0.4% bisacrylamide. The cathode buffer (upper chamber) contained 0.1 M Tris, 0.1 M Tricine, and 0.1% (w/v) SDS; the anode buffer contained 0.2 M Tris·Cl, pH 8.9. Gels were run at 80 watts (for a 33 × 39-cm gel) for 2.5 h. Products were visualized by using a PhosphorImager and quantified by using ImageQuant software.

RESULTS

Rationale

If the integrity of interface I (Fig. 1*C*) is necessary for virus viability, then disruption of this interface by changing residues on the back of the thumb subdomain (R455A,R456A) or the palm subdomain (D349R) should produce virus with equivalent phenotypes. This is not observed (4). It is possible that changing a single residue on the back of the palm is not sufficient to disrupt this interface. Therefore, we engineered a 3Dpol derivative in which aspartic acids 339 and 349 and serine 341 were all changed to alanines (D339A,S341A,D349A). This derivative will be referred to as the palm mutant. We have evaluated this mutant in biological and biochemical assays to determine the function for interface I in virus multiplication. To compare the data obtained in this study to that from others, we have reconstructed and evaluated the R455A,R456A 3Dpol derivative. This derivative will be referred to as the thumb mutant.

Biological Analysis of Interface I Mutants: Interface I Mutants Do Not Display Equivalent Phenotypes

To evaluate the viability of virus containing mutations in interface I, we performed an infectious center assay. HeLa cells were transfected with wild-type or mutant genomes, and these cells were plated at various dilutions on a HeLa cell monolayer. After adsorption, cells were covered with agar media and incubated at 37 °C for 3 days. After removal of the agar, remaining cells were stained with crystal violet. Without dilution, wild-type and palm mutant virus spread throughout the entire monolayer (Fig. 2). As expected, thumb mutant virus did not spread (Fig. 2) (4, 8). By evaluating higher dilutions of the palm mutant, it becomes clear that this mutant virus is somewhat debilitated relative to wild-type virus (Fig. 2). The titer of the palm mutant virus does not appear to be affected because the number of plaques observed is equivalent to wild-type virus (Fig. 2). However, the kinetics of multiplication of the palm mutant virus is reduced because the size of the plaques is significantly smaller than observed for wild-type virus (Fig. 2). These data are consistent with the hypothesis that the lethal phenotype observed for the thumb mutant virus is independent of the integrity of interface I.

To determine whether these phenotypes reflected defects to RNA synthesis, we evaluated the mutants by using a subgenomic replicon assay (9). The replicon contains a luciferase gene in place of the capsid-coding sequence, permitting RNA synthesis to be monitored indirectly by measuring luciferase activity (Fig. 3*A*) (9). Because the initial production of luciferase is dependent upon translation of transfected RNA, this assay can also provide an indication of whether RNA stability or translational efficiency is affected by the introduced mutations. The thumb mutant was incapable of RNA synthesis, and the palm mutant showed a decreased rate of RNA synthesis at 37 °C (Fig. 3*B*). By lowering the culture temperature to 30 °C, we were able to completely reverse the phenotype observed for the palm mutant relative to the wild-type control (Fig. 3*C*). Although we were not able to plaque the thumb mutant virus under these conditions, the replicon assay showed a very slow, steady accumulation of RNA for this mutant (data not shown

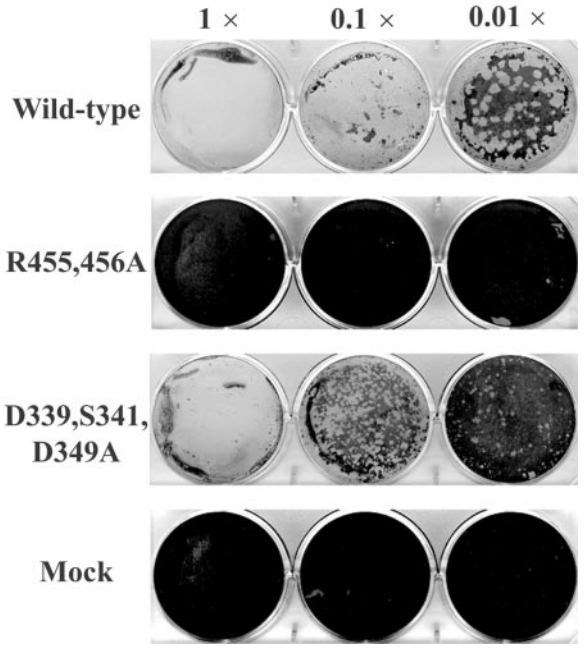

FIG. 2. **Mutations in interface I do not produce equivalent phenotypes.** HeLa cells were transfected with wild-type poliovirus RNA, RNA containing the indicated mutations in 3Dpol, or no RNA (mock transfection). Serial dilutions were then plated onto a monolayer of untransfected HeLa cells. Plates were covered with agar media and incubated at 37 °C for 3 days. Shown here are the plates after removal of the agar overlay and staining with crystal violet. Although virus containing mutations to the thumb subdomain (*R455,456A*) has a lethal growth phenotype, virus containing mutations to the palm subdomain (*D339,S341,D349A*) is viable with a slow-growth phenotype.

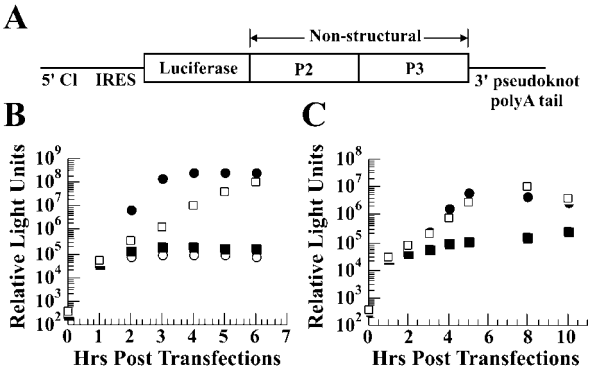

FIG. 3. **Interface I is required for RNA synthesis.** *A*, the subgenomic replicon employed has the capsid-coding region replaced by a luciferase reporter gene. Luciferase is released from the polyprotein by normal processing of 2A protease. The 5′ cloverleaf (*Cl*), the internal ribosomal entry site (*IRES*), the 3′ pseudoknot, and the poly(A) tail remain intact. *B*, analysis at 37 °C. HeLa cells were transfected with a subgenomic replicon RNA containing the wild-type sequence in the presence of 2 mM GdnHCl (○) or wild-type sequence in the absence of GdnHCl (●). GdnHCl is a reversible inhibitor of poliovirus RNA replication; therefore, the luciferase activity measured in the presence of GdnHCl is the result of translation of the input RNA. In the absence of GdnHCl, transfections were also performed using replicons containing mutations in either the thumb subdomain (R455A,R456A) (■) or palm subdomain (D339A,S341A,D349A) (□). Transfection reactions were incubated at 37 °C. At various times after transfection, cells were processed (see "Experimental Procedures") and luciferase activity evaluated. The thumb mutant replicon is incapable of RNA synthesis, whereas the palm mutant replicon has a decreased rate of RNA synthesis compared with the wild-type replicon in the absence of GdnHCl. *C*, analysis at 30 °C. The difference between the palm mutant and the wild-type replicon was completely eliminated by reducing the temperature. Interestingly, the thumb mutant appears to be replicating at a very slow, but observable, rate at the reduced temperature.

and Fig. 3*C*). RNA stability and translation did not appear to be affected for any of the mutant replicons tested in this assay, as wild-type and mutant replicons displayed the same level of luciferase activity at the 1-h time point (Fig. 3, *B* and *C*).

Biochemical Analysis of Interface I Mutants

The Thumb Mutant Is Impaired for Capsid Precursor Processing—Although the overall stability and translatability of genomes encoding mutations in interface I were equivalent to wild-type RNA, it was possible that these mutations caused problems with processing of the viral proteins required for replication. To test this possibility, a cell-free translation/replication system was employed (13). The system was programmed with wild-type or mutant genomes, and reactions were performed for 3 h at 34 °C in presence of [^{35}S]methionine. Labeled proteins were visualized by phosphorimaging after separation by SDS-PAGE (Fig. 4*A*). Consistent with the replicon data, both mutants produced levels of protein equivalent to wild-type control (Fig. 4*A*). All of the expected precursor and processed forms of the capsid (P1, VP0, VP1, and VP3) and nonstructural (P3, P2, 3BCD, 3CD, 3D, 3C, 3AB, 2BC, 2C, and 2A) proteins were observed (Fig. 4*A*). Processed and precursor proteins containing the palm mutant 3D subunit showed altered mobility owing to the change in charge of this protein caused by removal of the two carboxylate side chains (Fig. 4*A*). Interestingly, the amount of VP0/VP3 precursor protein produced by the thumb mutant was elevated relative to the wild-type control (Fig. 4*A*, *lane 3*), suggesting a defect to processing of this precursor. Consistent with this observation, the amount of VP3 protein was reduced (Fig. 4*A*, *lane 3*). A corresponding reduction in VP0 was not as evident for the thumb mutant owing to the comigration of this protein with the 2C protein (Fig. 4*A*, *lane 3*). We conclude that the reduced accumulation of RNA observed for interface I mutants is not a reflection of reduced, altered, or aberrant processing of the viral nonstructural proteins.

The Thumb Mutant Is Defective, and the Palm Mutant Is Impaired for RNA Synthesis—The cell-free translation/replication system facilitates direct evaluation of RNA synthesis (13). Translation is performed in the presence of 2 mM guanidine, an inhibitor of RNA synthesis. Initiation complexes are isolated by centrifugation, RNA synthesis can then be evaluated after suspension of the pelleted complexes in buffer containing nucleoside triphosphates. Use of [α-^{32}P]CTP permits visualization of the RNA product after agarose gel electrophoresis by using a PhosphorImager. The interface I mutants were evaluated by using this system; the results are shown in Fig. 4*B*. Although the palm mutant was capable of producing genomic RNA, the thumb mutant was not. The palm mutant exhibited a 4-fold reduction in the quantity of genomic RNA produced relative to the wild-type control. This observation is consistent with the reduction in the rate of RNA accumulation inferred from the subgenomic replicon data (Fig. 3*B*).

Both Thumb and Palm Mutants Exhibit Equivalent Defects in Oligomerization Capacity—The disparity in phenotypes observed for the thumb and palm mutants suggested the possibility that the interaction domain observed crystallographically (1) might not be responsible for the oligomerization of polymerase observed biochemically. To exclude this possibility, we expressed the thumb and palm polymerase derivatives in *E. coli*, purified the enzymes, and evaluated their ability to oligomerize in solution by using the filter-binding assay established to monitor RNA binding by and oligomerization of 3Dpol (2). For this assay, equilibrated mixtures of protein and labeled nucleic acid are pulled by vacuum through a stack of three membranes: polysulfone, nitrocellulose, and nylon. Complexes retained on the polysulfone membrane are selected based upon

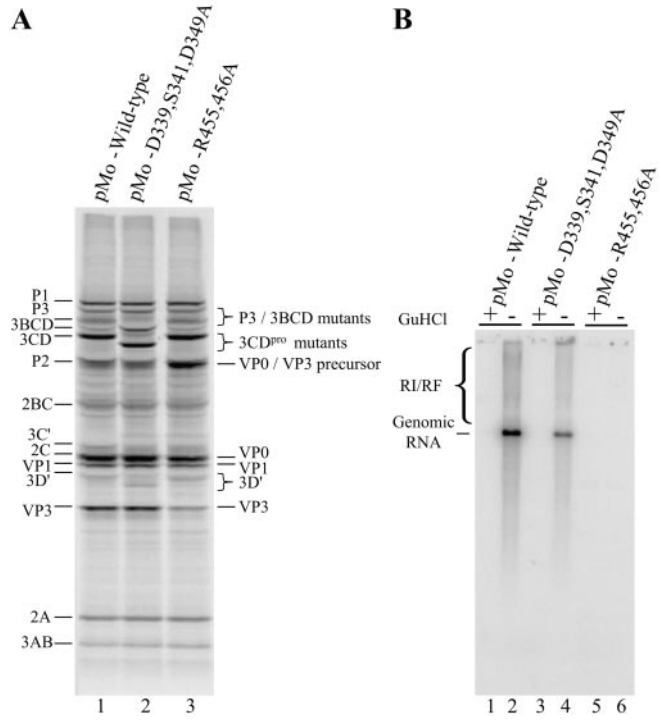

FIG. 4. **The thumb surface of interface I is required for efficient processing of the VP0/VP3 capsid precursor and RNA synthesis.** *A*, reactions containing the wild-type poliovirus genome (*lane 1*) or the interface I mutant genomes (*lanes 2* and *3*) (50 μg/ml) were incubated in HeLa S10 translation-replication reactions containing [^{35}S] methionine at 34 °C for 3 h. Radiolabeled proteins were separated by electrophoresis in a 9–18% SDS-PAGE gel. Radiolabeled proteins were detected by phosphorimaging. Translation and processing of the replication proteins appears equivalent for all of the genomes. Processing of the capsid precursor, VP0/VP3, however, appears to be inefficient for the thumb mutant genome reaction (compare *lane 3* with *lanes 1* and *2*). *B*, following 3 h of translation, preinitiation RNA replication complexes were isolated from reactions containing the indicated viral mRNAs and 2 mM GdnHCl. Preinitiation RNA replication complexes were incubated at 37 °C for 60 min in reactions containing [α-^{32}P]CTP in the presence (*lanes 1*, *3*, and *5*) and absence (*lanes 2*, *4*, and *6*) of 2 mM GdnHCl. RNA products were separated by gel electrophoresis in 1% agarose, and radiolabeled RNA was detected by phosphorimaging. The genome containing the thumb mutations fails to synthesize any genomic RNA or show any signs of negative strand RNA synthesis (the replicative intermediate (*RI*) and the replicative form (*RF*)) (*lane 6*). The wild-type and palm mutant genomes (*lanes 2* and *4*, respectively) show evidence for the formation of all three types of RNA. The amount of RNA synthesized by the palm (*lane 4*) is 4-fold lower than the wild-type genome (*lane 2*).

size (0.45-μm cut-off), as neither protein nor nucleic acid bind to this membrane. In the case of 3Dpol, these complexes should contain on the order of 100 molecules given the dimensions of the enzyme. All soluble protein-nucleic acid complexes will bind to the nitrocellulose. Any unbound nucleic acid will bind to the nylon, thus increasing the accuracy of quantification. Each polymerase was evaluated at varying concentrations (0.1–5 μM) with an end-labeled rU_{30} oligonucleotide (10 nM). Complexes bound to each membrane were visualized by phosphorimaging (Fig. 5*A*), and those bound to the polysulfone, the nitrocellulose, or both were quantified by using the ImageQuant software from Amersham Biosciences (Fig. 5, *B–D*). As the concentration of wild-type 3Dpol was increased, an accumulation of very large complexes was observed (Fig. 5*B*). These large complexes formed at the expense of the smaller complexes (Fig. 5*C*). In contrast, over the same concentration range, neither interface mutant formed very large complexes (Fig. 5*B*); essentially all of these complexes were bound to the nitrocellulose membrane (Fig. 5*C*). The overall RNA-binding affinity was evaluated by plotting the sum of all bound species as a function of 3Dpol concentration and shown to be the same for all derivatives (Fig. 5*D*). In addition, in contrast to previous reports (2–4), cooperative RNA binding was not observed (Fig. 5, *B–D*). We conclude that oligomerization observed biochemically is the result, at least in part, of interface I observed crystallographically. The finding that neither mutant forms large polymerase fibers suggests that the RNA synthesis phenotype is not related to polymerase fiber formation.

Interface I Is Dispensable for Polymerase Functions Required for Nucleotide Incorporation—To begin to define the function of the back of the thumb, we constructed, expressed and purified two additional thumb mutants (R455S,R456S and R455D, R456D). Serine was introduced to test the possibility that exposure of even a small aliphatic moiety would alter the conformation of the thumb. Aspartic acid was introduced to completely disrupt any residual interaction between the thumb and palm that might remain, with the hope of making any biochemical differences more obvious. The active fraction of each purified enzyme preparation was similar and ranged from 96.5 to 98.5% (see "Active site titration" in Table II). Consistent with the results obtained by using the filter-binding assay, the stability of each polymerase derivative with a primer/template substrate that mimics an elongation intermediate varied less than 2-fold from the wild-type value (see "k_{off} 3Dpol-sym/sub" in Table II). Each derivative was more resistant to thermal inactivation than the wild-type enzyme (see "Thermal inactivation" in Table II). This observation may suggest that the observed inactivation *in vitro* is related to polymerase multimerization. The rate of nucleotide incorporation of each derivative was within 80% of the value measured for wild-type 3Dpol (see "Rate of AMP incorporation" in Table II). Finally, consistent with previous findings (4), interface I mutants display differences in poly(rU) polymerase activity relative to the wild-type enzyme. The thumb derivatives exhibit a 1.5–3-fold reduction in poly(rU) polymerase activity (see "Poly(rU) polymerase" in Table II); the palm derivative exhibits a 1.7-fold increase in poly(rU) polymerase activity (see "Poly(rU) polymerase" in Table II). We have shown that the rate-limiting step measured by using this assay is template switching (5). Therefore, it is difficult to reach any conclusions from these data when subtle changes are observed. Taken together, these data suggest that all of the functions required for processive elongation of RNA are retained by polymerases that are incapable of forming fibers.

Mutations on the Back of the Thumb of 3Dpol Interfere with VPg Uridylylation—Because elongation does not appear to be affected by interface I mutations, we focused our attention on the initiation reaction. Initiation of poliovirus negative- and positive-strand RNA synthesis requires, minimally, the polymerase, the 22-amino acid peptide primer (VPg), and a template (18). For negative-strand RNA synthesis, it has been suggested that the template may either be poly(rA) tail at the 3′ end of viral RNA (18) or a 61-nt stem loop RNA located in 2C-coding sequence (Fig. 6*A*) (19). We will refer to this 61-nt cis-acting replication element (cre) (20) as oriI (internal origin of replication). By using VPg, oriI, and UTP, 3Dpol can activate a VPg tyrosine for nucleophilic attack on the α-phosphorus of UTP to form VPg-pU, which, in turn, is used as the source of the nucleophile for addition of a second uridylate residue to form VPg-pUpU (Fig. 6*B*) (19). Uridylylation is templated by a single adenylate residue located in the loop of oriI (see *boldface A* in Fig. 6*A*) by using a slide-back mechanism (21) similar to that described by Salas and colleagues (22) for bacteriophage Φ29. This reaction is stimulated by more than 20-fold by adding viral protein 3CD to

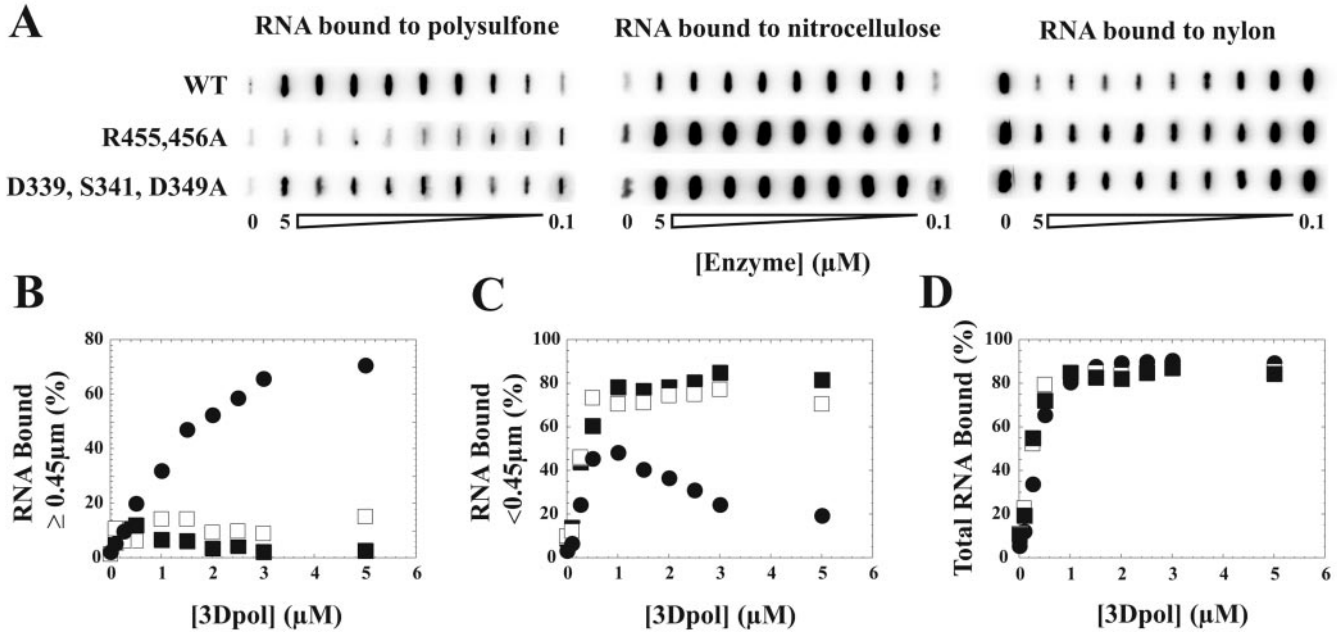

FIG. 5. **Both interface I mutants are defective in fiber formation.** Radiolabeled rU_{30} was incubated in reaction buffer with varying concentrations of the indicated 3Dpol derivatives for 30 min on ice. A slot-blot apparatus was then used to analyze the reactions (see "Experimental Procedures"). *A*, shown are the phosphorimages of the membranes obtained from this analysis; the polysulfone membrane retains all complexes ≥0.45 μm (~100 3Dpol molecules), the nitrocellulose membrane binds protein-RNA complexes <0.45 μm and any free protein, and the nylon membrane binds all of the free RNA. *WT*, wild-type 3Dpol; *R455,456A*, 3Dpol-R455A,R456A; *D339,S341,D349A*, 3Dpol-D339A,S341A,D349A. *B*, quantification of the protein-RNA complexes on the polysulfone membrane shows that mutations to the thumb and palm subdomains preclude formation of long 3Dpol fibers. *C*, quantification of the protein-RNA complexes bound to the nitrocellulose membrane. *D*, evaluation of the total RNA bound by each 3Dpol derivative reveals that both mutants bind RNA. It is evident that disruption of interface I does not perturb the affinity for RNA relative to the wild-type enzyme. ●, wild-type 3Dpol; ■, 3Dpol-R455A,R456A; □, 3Dpol-D339A,S341A,D349A.

TABLE II
Ability of 3Dpol derivatives to elongate RNA

3Dpol derivatives	Active site titration[a]	k_{off} 3Dpol-sym/sub[a]	Thermal inactivation[a]	Rate of AMP incorporation[a]	Poly(rU) polymerase[a]
	%	s^{-1} ($\times 10^{-4}$)	s^{-1} ($\times 10^{-3}$)	s^{-1}	pmol/min/μg
WT[b]	96.5 ± 3.5	5.9 ± 0.2	15 ± 1.0	72.4 ± 4.4	634 ± 36
R455A,R456A	96.6 ± 3.4	7.7 ± 0.2	7.7 ± 1.0	66.5 ± 8.5	428 ± 71
R455S,R456S	97.3 ± 2.7	9.4 ± 0.3	8.0 ± 0.4	55.3 ± 2.4	296 ± 43
R455D,R456D	98.5 ± 1.5	6.2 ± 0.2	4.1 ± 0.4	65.6 ± 4.6	224 ± 49
D339A,S341A,D349A	97.0 ± 3.0	4.6 ± 0.4	5.6 ± 0.2	57.9 ± 7.9	1074 ± 170

[a] See "Experimental Procedures" for a description of how each assay was performed.
[b] wild type.

the reaction mixture (19). The mechanistic basis for this observation is not known. Protein 3CD is a precursor form of the 3C protease and 3D polymerase. This protein has protease activity and RNA binding activity but lacks polymerase activity (23, 24). Although it is currently not clear that oriI serves as the site for initiation *in vivo*, the specificity of this reaction is consistent with this role (19, 21, 25).

We evaluated the ability of each derivative to catalyze oriI-dependent, 3CD-stimulated uridylylation of VPg. In these reactions, the incorporation of [α-^{32}P]UTP into VPg-pUpU is monitored by SDS-PAGE using a Tris-Tricine buffer system. The phosphorimage of a typical gel is shown in Fig. 6*C*. Both VPg-pU and VPg-pUpU can be resolved from the labeled UTP, which can be retained on the gel to permit accurate quantification. Interestingly, all of the thumb mutants are significantly impaired for uridylylation (Fig. 6*C*, *lanes 2–4*) relative to wild-type 3Dpol (Fig. 6*C*, *lane 1*). The palm mutant does not exhibit a significant difference relative to wild-type 3Dpol (Fig. 6*C*, *lane 5*). Quantification of the data revealed that there was an 8-fold reduction in uridylylation for the R455A,R456A and R455S,R456S derivatives and a 108-fold reduction in uridylylation for the R455D, R456D derivative relative to wild-type 3Dpol, and the palm mutant was essentially unaffected (Fig. 6*D*). At 30 °C, the observed difference for the R455A,R456A and R455S,R456S derivatives diminished to only 3-fold without any impact on the extent of the defect observed for the R455D,R456D derivative (Fig. 6*E*). The diminution in the magnitude of the defect to uridylylation at 30 °C for the R455A,R456A derivative may explain the ability of the R455A,R456A replicon to produce RNA at 30 °C (Fig. 3*C*). By omitting 3CD from the reaction, it became clear that the primary effect of the thumb mutations was on the capacity of these derivatives to be stimulated by 3CD (Fig. 6*F*). In the absence of 3CD, the thumb derivatives catalyzed uridylylation at a rate that was within 2–3-fold of the value for the wild-type enzyme, suggesting that the intrinsic ability of these enzymes to catalyze uridylylation is not affected. Comparison of the data presented in Fig. 6*D* with that presented in Fig. 6*F* showed that 3CD stimulated the wild-type enzyme 46-fold, the R455A,R456A and R455S,R456S enzymes 13-fold, and the R455D,R456D derivative not at all.

We also performed experiments to rule out other trivial explanations for the observed effects on the uridylylation reaction. The linearity of the reaction was unchanged (data not shown). In addition, the observed reduction was not because of significant changes in the $K_{0.5}$ values for UTP (data not shown). However, there was a subtle difference between the VPg $K_{0.5}$

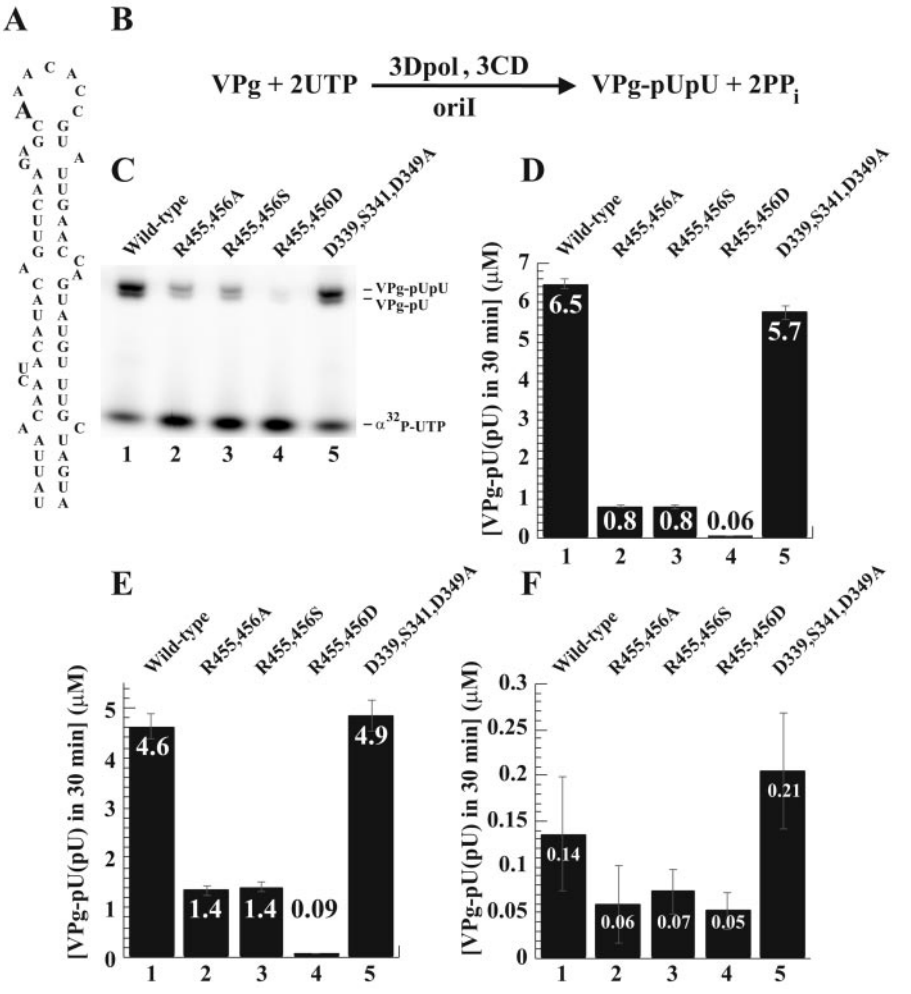

FIG. 6. **The thumb surface, but not the palm surface, of interface I is required for oriI-templated VPg uridylylation.** *A*, the predicted secondary structure for the 61-nt oriI, the template for VPg uridylylation producing VPg-pU and VPg-pUpU. The templating "A" appears in a *larger point size*. *R455, 456A*, 3Dpol-R455A,R456A; *R455,456S*, 3Dpol-R455S,R456S; *R455,456D*, 3Dpol-R455D,R456D; *D339,S341,D349A*, 3Dpol-D339A,S341A,D349A. *B*, 3Dpol can uridylylate VPg, a 22-amino acid peptide. In the presence of 3CD, this product is increased more than 20-fold. *C*, reaction mixtures contained 1 μM 3D, 0 or 1 μM 3CD, 1 μM 61-nt oriI, 50 μM VPg, 10 μM UTP, and 0.004 μM [α-^{32}P]UTP. Wild-type 3Dpol or 3Dpol containing the indicated interface I mutations were incubated in reaction mixtures at either 37 or 30 °C for 30 min. Shown here is a representative 15% Tris-Tricine gel used to separate the singly and doubly uridylylated VPg products from the unincorporated [α-^{32}P]UTP. *D*, quantification of reaction products in the presence of 3CD shows that 3Dpol derivatives containing mutations in the thumb subdomain (*bars 2–4*) are unable to be stimulated to the same level as the wild-type polymerase (*bar 1*), whereas the 3Dpol derivative containing mutations in the palm subdomain (*bar 5*) displayed essentially wild-type levels of uridylylation. Reactions were performed at 37 °C. *E*, at 30 °C, the magnitude of the defect for the thumb derivative is reduced. *F*, quantification of the uridylylation reaction products in the absence of 3CD stimulation shows that there is no greater than a 2-fold difference between the interface I derivatives (*bars 2–5*) and the wild-type polymerase (*bar 1*). Reactions were performed at 30 °C.

values for the thumb derivative (12 μM) relative to wild-type 3Dpol (6 μM) (Fig. 7). This difference cannot account for the effects observed here, as VPg was employed at a concentration of 50 μM. This concentration of VPg is sufficient to saturate the thumb mutant.

Finally, to corroborate the data obtained by using the reconstituted system, we evaluated the accumulation of VPg-pU(pU) in the cell-free translation/replication system. As expected, the thumb mutant was incapable of uridylylating VPg in this system as well (Fig. 8). It should be noted that the radiolabeled products that appear in the presence of guanidine reflect the labeling of cellular components in the reactions.

Evidence for an Interaction between the Back of the Thumb of 3Dpol and an Undefined Domain of Protein 3C—The simplest interpretation of the observation that the thumb mutants cannot be stimulated by 3CD is that a physical interaction exists between 3Dpol and 3CD that permits uridylylation-competent complexes to form more efficiently and/or product to form faster. The extent of the effect of uridylylation observed with the thumb derivatives was consistent with predictions made by evaluating the structure of interface I (Fig. 1*C*). In particular, the R455S,R456S derivative was stimulated to a greater extent than the R455D,R456D derivative. Therefore, we hypothesized that the interaction of 3Dpol with 3CD was mediated by an interaction with the back of the palm of the 3D domain located on the 3CD protein. To test this hypothesis, we subcloned the original thumb and palm mutations into our 3CD expression vector, expressed, purified, and characterized these proteins in the uridylylation assay. Both the thumb and palm mutant 3CD derivatives were active in this reaction (Fig. 9). To determine

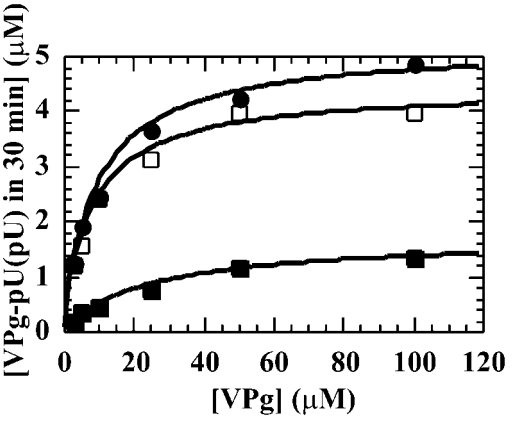

FIG. 7. **The defect to oriI-templated uridylylation is unrelated to VPg binding.** Uridylylation reactions were performed as described under "Experimental Procedures." VPg was titrated from 0 to 100 μM in reactions that contained either wild-type 3Dpol or 3Dpol containing the indicated interface I mutations. Reactions were performed for 30 min at 30 °C. The amount of VPg uridylylated was plotted as a function of VPg concentration. Shown is a hyperbolic fit for each set of data. The following $K_{0.5}$ values were calculated: wild-type 3Dpol (●), 6.6 μM; 3Dpol-R455A,R456A (■), 11.4 μM; and 3Dpol-D339A,S341A,D349A (□), 5.6 μM.

whether the stimulatory activity of 3CD resided in the 3Dpol domain of this protein, we constructed a 3C expression vector, expressed, purified, and characterized this protein in the uridylylation assay. To our surprise, 3C was capable of stimulating uridylylation of VPg within 2-fold of that observed for 3CD

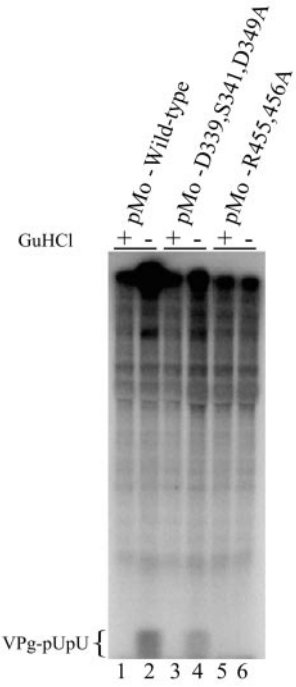

FIG. 8. **Mutations to the thumb surface of interface I, but not mutations to the palm surface, affect uridylylation of VPg in cell-free translation-replication reactions.** Following 3 h of translation, preinitiation RNA replication complexes were isolated from reactions containing the indicated viral mRNAs and 2 mM GdnHCl. Preinitiation RNA replication complexes were incubated at 37 °C for 60 min in reactions containing [α-^{32}P]UTP in the presence (*lanes 1*, *3*, and *5*) and absence (*lanes 2*, *4*, and *6*) of 2 mM GdnHCl. Products were separated by using a 10% polyacrylamide Tris-Tricine gel. The genome containing the thumb mutations does not produce any detectable uridylylated VPg (*lane 6*), whereas the palm mutant does form a significant amount of VPg-pUpU (*lane 4*). The product is approximately one-third the amount produced by the wild-type genome (*lane 2*).

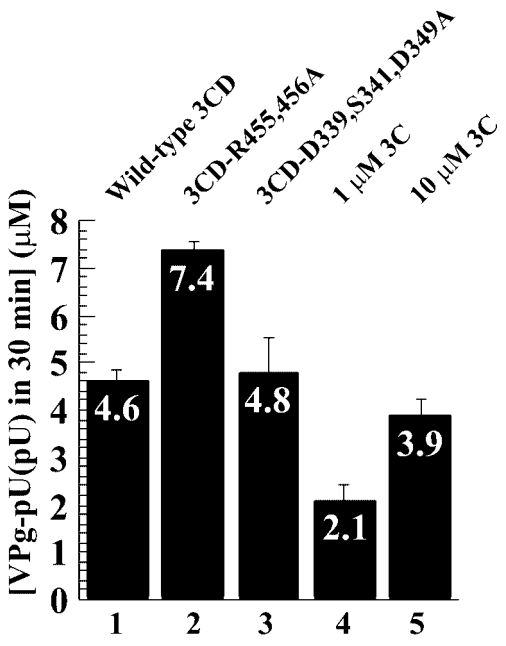

FIG. 9. **The stimulatory activity of 3CD resides in the 3C domain of this protein.** Reactions contained 1 μM wild-type 3CD or 3CD containing the indicated interface I mutations in the 3D domain, 1 μM 3C, or 10 μM 3C. Reactions were performed for 30 min at 30 °C. Quantification of the reaction products showed that neither the thumb (*bar 2*) nor palm mutations (*bar 3*) reduce 3CD stimulation of the reaction relative to wild-type 3CD (bar 1). Deletion of the entire polymerase domain from 3CD shows that 3C is capable of stimulating the uridylylation reaction (*bar 4*). Raising the concentration of 3C to 10 μM increases stimulation to a level comparable with that of 3CD (*bar 5*). *R455,456A*, R455A,R456A; *D339,S341,D349A*, D339A,S341A,D349A.

(Fig. 9, *bar 4*). By increasing the concentration of 3C, we could increase the stimulation to the level observed for 3CD (Fig. 9, *bar 5*). These data suggest that 3C contains all of the determinants for stimulation, *i.e.* formation of an activated uridylylation complex. However, the 3Dpol domain of 3CD appears to contribute to the overall stability of this complex.

Consistent with the possibility for an interaction between the back of the thumb of 3Dpol and some region of 3C is the observation that the 3CD-R455A,R456A derivative is more active than others (Fig. 9, *bar 2*). This derivative should not have 3CD-3CD interactions competing with formation of 3Dpol-3CD interactions required to form the activated uridylylation complex.

DISCUSSION

The crystal structure for 3Dpol was the first available for an RNA-dependent RNA polymerase (1). This structure confirmed predictions that the overall fold of all nucleic acid polymerases is similar but also identified several unique features for this enzyme. In particular, a polymerase lattice is formed by head-to-tail interaction of polymerase subunits (interface I) and interaction between the resulting polymerase fibers (interface II). Molecular genetic evidence supported a biological function for these fibers (8). Biochemical studies suggested that the ability to form fibers facilitated complete coating of template RNA, possibly a prerequisite for activity, and explained the cooperativity observed with respect to polymerase activity (2) and RNA binding (2–4). These observations led to the prediction that all RdRPs may function similarly to 3Dpol (26). Indeed, evidence for oligomerization of the RdRP from hepatitis C virus, NS5B, has been pursued rather aggressively (27, 28). Given that DNA-dependent DNA and RNA polymerases do not need to oligomerize for activity or nucleic acid binding (29–31) and a single subunit of an RdRP has all of the elements present in these enzymes (1), it has been difficult to reconcile the observation that RdRP oligomerization is required for activity and/or RNA binding.

Although disruption of interface I by altering residues on the back of the thumb of 3Dpol is lethal to the virus (4, 8), disruption of interface I by altering residues on the back of the palm is not (4). Our palm mutant (D339A,S341A,D349A) was predicted to be as disruptive as the thumb mutant (R455A,R456A) reported previously (Fig. 1*C*). Interestingly, this palm mutant also supported virus viability (Fig. 2), in addition to translation (Figs. 3 and 4*A*) and genome replication (Figs. 3 and 4*B*). Moreover, the finding that both the palm and thumb mutants are incapable of forming long fibers (Fig. 5) suggests that the capacity to form fibers is not essential for virus multiplication. In addition, this observation strengthens the argument that the lethal phenotype associated with the thumb mutant is unrelated to formation of polymerase fibers.

The thumb mutant was not capable of processing the VP0/VP3 junction as well as the wild type (Fig. 4*A*). Clearly, this phenotype must be a reflection of an alteration in 3CD protease activity. It is known that 3CD is more active at capsid precursor processing *in vitro* than 3C (32, 33). Interestingly, processing of the VP0/VP3 junction by 3CD requires a cellular cofactor (34). It is possible that one function for the back of the thumb may be to interact with this cellular cofactor. Although this processing defect will limit or even preclude virus spread, this defect should not have any impact on genome replication. Proc-

essing of the nonstructural proteins in the thumb mutant was not affected (Fig. 4*A*). However, the thumb mutant replicon failed to produce RNA (Fig. 3), and the thumb mutant RNA failed to support replication in the cell-free translation/replication system (Fig. 4*B*). We concluded that the residues on the back of the thumb play a unique, undefined role in viral RNA synthesis.

None of the thumb mutants exhibited any significant alteration in RNA binding properties (Fig. 5 and Table II), and cooperative binding to RNA was not observed by using the RNA oligonucleotide employed in this study (Fig. 5D). The fraction of enzyme active in each preparation, the stability of each polymerase elongation complex, the thermal stability of each polymerase derivative, and the observed rate of nucleotide incorporation for each derivative were essentially unchanged relative to wild-type 3Dpol (Table II). The nucleic acid substrate employed in this study has been shown to predict biological phenotypes and is thought to recapitulate the elongation phase of viral RNA synthesis (16). A previous study of interface I mutants showed minimal to substantial changes in RNA binding and/or elongation for derivatives analogous to those presented here (4). The magnitude of the effect was dependent upon the RNA ligand/substrate employed. Because these two studies were performed under substantially different conditions with different RNA ligands/substrates, it is not possible to explain the differences in outcome. Taken together, our data support the conclusion that changes in biochemical properties required for RNA synthesis do not explain the lethal phenotype of the thumb mutant.

Consistent with previous studies (4), a modest reduction in the poly(rU) polymerase activity was observed for the thumb mutants (Table II). For the R455A,R456A derivative, a 1.5-fold reduction was noted (Table II). We have shown that the rate-limiting step measured by using the poly(rU) polymerase assay is template switching (5). Template switching is thought to be the primary mechanism for homologous recombination in poliovirus (35, 36). Because the recombination frequency for poliovirus ranges from 0.01 to 0.1/genome (35, 36), a 50% reduction in this value is likely too small to cause the lethal phenotype observed for the R455A,R456A mutant virus.

The elongation phase of viral genome replication appeared fine, so we turned our attention to the initiation phase. It has been suggested that the cis-acting replication element located in the 2C-coding region of the poliovirus genome (20) acts as an internal origin of replication (oriI) (19). The thought is that 3Dpol would initiate VPg-primed RNA synthesis at this internal site to produce VPg-pUpU, which, in turn, would be transferred to the 3′ end of viral RNA and extended by 3Dpol to produce full-length, VPg-linked RNA. An *in vitro* system recapitulating the VPg uridylylation step was recently reported (19). The basal reaction is stimulated substantially by the presence of the viral 3CD protein; however, the molecular basis for this stimulation is not known. Interestingly, when the thumb mutants were evaluated in this assay, we observed a substantial reduction (8–100-fold at 37 °C) in the efficiency of VPg uridylylation (Fig. 6). The affinity for VPg was not changed (Fig. 7). The basal activity of each derivative was within ~2-fold of the wild-type value (Fig. 6). In addition, a defect to VPg uridylylation was also observed in the cell-free translation/replication system (Fig. 8). These data provided an intellectually satisfying explanation for the phenotype associated with the thumb mutant virus.

By mutating the back of the thumb of 3Dpol, the VPg uridylylation reaction could not be stimulated by 3CD (Fig. 8). The simplest explanation was that a physical interaction between 3Dpol and 3CD was required to simulate VPg uridylylation and that this interaction was lost by altering the back of the thumb. Surprisingly, this interaction did not occur between the back of the thumb of 3Dpol and the back of the palm of the 3Dpol domain of 3CD as the 3Dpol palm domain of 3CD could be modified without consequence to the stimulatory capacity of 3CD (Fig. 9). In fact, the entire 3Dpol domain of 3CD could be deleted and the stimulatory activity retained (Fig. 9). Our working hypothesis is shown in Fig. 10*A*. The activated uridylylation complex forms sequentially; 3CD binds to oriI and recruits 3D to the site on oriI that serves as a template for uridylylation. Recruitment is mediated by an interaction between the back of the thumb of 3Dpol and an undefined domain of 3C. Although an interaction between 3D and 3CD has been shown by using the yeast two-hybrid system, these studies did not identify an interaction between 3D and 3C (7). It is possible that the 3D-3C interaction requires RNA for maximal stability.

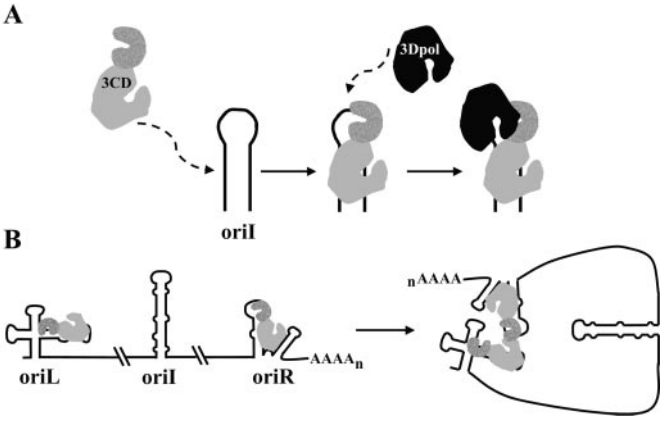

FIG. 10. **The interaction between 3D and 3C may be required to establish the VPg uridylylation complex and other complexes required for poliovirus genome replication.** *A*, VPg uridylylation complex. Protein 3CD (*gray molecule*) binds to oriI and subsequently recruits polymerase to this complex by using an interaction with the back of the thumb of 3Dpol. In this model, the 3C domain of 3CD is *speckled*. The location of the interaction surface of 3C is currently not known. *B*, initiation of negative-strand RNA synthesis. Protein 3CD not only binds to oriI but also binds to oriL and oriR (cis-acting replication elements at the 5′ and 3′ ends of viral RNA, respectively (Refs. 24 and 39)). It is possible that an interaction between 3CD molecules (3C from one molecule interacting with 3D from a second molecule) facilitates recruitment of the 3′ end to the 5′ end for "circularization" of the genome. Protein 3CD-mediated circularization of the poliovirus genome has been suggested previously as a prerequisite for negative-strand RNA synthesis (37, 38).

The R455A,R456A derivative exhibited an 8-fold reduction in uridylylation efficiency relative to wild-type 3Dpol in the reconstituted system (Fig. 6, *D* and *E*). In contrast, this mutant fails to produce uridylylated VPg in the cell-free extract (Fig. 8). This difference may reflect the inability to detect the first round of VPg uridylylation and may indicate that genomes produced within replication complexes serve as the primary templates for VPg uridylylation observed in extracts. This scenario would also explain the observation that the palm mutant shows no defect to VPg uridylylation in the reconstituted system but a subtle defect in the cell-free extract (Fig. 8) on par with the defect observed for RNA synthesis (Fig. 3*B*).

Is the magnitude of the defect to VPg uridylylation observed for the thumb mutant in the reconstituted system sufficient to account for the complete inability of this mutant to produce viral RNA? It is possible that the 3D-3C interaction is required for other aspects of the genome-replication process. For exam-

ple, it has been suggested that poliovirus RNA must "circularize" via protein-protein interactions for negative-strand RNA synthesis (37, 38). Protein 3CD and cellular factors have been implicated in this protein bridge. It is known that 3CD binds to the cis-acting elements at the 5′ (oriL) and 3′ (oriR) ends of the viral genome (24, 39). As shown in Fig. 10*B*, it is possible that the ability of 3CD to function in genome circularization requires the 3D-3C interaction. This possibility would explain the severity of the defect associated with the thumb mutant. Additional studies will be required to investigate this possibility.

Although the palm mutant virus was viable, this virus did not grow as well as wild-type virus (Fig. 2). The defect to this virus was attributed to a modest reduction in the kinetics of RNA synthesis (Figs. 3*A* and 4*B*). Interestingly, the defect to RNA synthesis observed for the palm mutant relative to wild type could be reversed completely by lowering the temperature (Fig. 3*B*), consistent with changes in the stability of protein-protein interaction. It is difficult to imagine that such an intricate interaction domain like interface I would arise fortuitously. It is possible that the phenotype observed for the palm mutant is a consequence of the inability of this mutant to form polymerase fibers. Additional studies of this mutant may reveal the true function for polymerase fibers.

Acknowledgments—We thank Brandon Bilohlavek for construction of the thumb mutant expression plasmids, Chong Ha for construction of 3CD expression plasmids and optimization of the purification protocol, and Mehul Suthar for construction of the pET26Ub-Chis plasmid.

REFERENCES

1. Hansen, J. L., Long, A. M., and Schultz, S. C. (1997) *Structure* **5,** 1109–1122
2. Pata, J. D., Schultz, S. C., and Kirkegaard, K. (1995) *RNA* **1,** 466–477
3. Beckman, M. T., and Kirkegaard, K. (1998) *J. Biol. Chem.* **273,** 6724–6730
4. Hobson, S. D., Rosenblum, E. S., Richards, O. C., Richmond, K., Kirkegaard, K., and Schultz, S. C. (2001) *EMBO J.* **20,** 1153–1163
5. Arnold, J. J., and Cameron, C. E. (1999) *J. Biol. Chem.* **274,** 2706–2716
6. Hope, D. A., Diamond, S. E., and Kirkegaard, K. (1997) *J. Virol.* **71,** 9490–9498
7. Xiang, W., Cuconati, A., Hope, D., Kirkegaard, K., and Wimmer, E. (1998) *J. Virol.* **72,** 6732–6741
8. Diamond, S. E., and Kirkegaard, K. (1994) *J. Virol.* **68,** 863–876
9. Herold, J., and Andino, R. (2000) *J. Virol.* **74,** 6394–6400
10. Gohara, D. W., Ha, C. S., Kumar, S., Ghosh, B., Arnold, J. J., Wisniewski, T. J., and Cameron, C. E. (1999) *Protein Expr. Purif.* **17,** 128–138
11. Gohara, D. W., Crotty, S., Arnold, J. J., Yoder, J. D., Andino, R., and Cameron, C. E. (2000) *J. Biol. Chem.* **275,** 25523–25532
12. Andino, R., Rieckhof, G. E., Achacoso, P. L., and Baltimore, D. (1993) *EMBO J.* **12,** 3587–3598
13. Lyons, T., Murray, K. E., Roberts, A. W., and Barton, D. J. (2001) *J. Virol.* **75,** 10696–10708
14. Barton, D. J., Morasco, B. J., and Flanegan, J. B. (1996) *Methods Enzymol.* **275,** 35–57
15. Barton, D. J., and Flanegan, J. B. (1997) *J. Virol.* **71,** 8482–8489
16. Arnold, J. J., and Cameron, C. E. (2000) *J. Biol. Chem.* **275,** 5329–5336
17. Carroll, S. S., Benseler, F., and Olsen, D. B. (1996) *Methods Enzymol.* **275,** 365–382
18. Paul, A. V., van Boom, J. H., Filippov, D., and Wimmer, E. (1998) *Nature* **393,** 280–284
19. Paul, A. V., Rieder, E., Kim, D. W., van Boom, J. H., and Wimmer, E. (2000) *J. Virol.* **74,** 10359–10370
20. Goodfellow, I., Chaudhry, Y., Richardson, A., Meredith, J., Almond, J. W., Barclay, W., and Evans, D. J. (2000) *J. Virol.* **74,** 4590–4600
21. Gerber, K., Wimmer, E., and Paul, A. V. (2001) *J. Virol.* **75,** 10979–10990
22. Meijer, W. J., Horcajadas, J. A., and Salas, M. (2001) *Microbiol. Mol. Biol. Rev.* **65(2),** 261–87.
23. Harris, K. S., Reddigari, S. R., Nicklin, M. J., Hammerle, T., and Wimmer, E. (1992) *J. Virol.* **66,** 7481–7489
24. Harris, K. S., Xiang, W., Alexander, L., Lane, W. S., Paul, A. V., and Wimmer, E. (1994) *J. Biol. Chem.* **269,** 27004–27014
25. Rieder, E., Paul, A. V., Kim, D. W., van Boom, J. H., and Wimmer, E. (2000) *J. Virol.* **74,** 10371–10380
26. O'Reilly, E. K., and Kao, C. C. (1998) *Virology* **252,** 287–303
27. Wang, Q. M., Hockman, M. A., Staschke, K., Johnson, R. B., Case, K. A., Lu, J., Parsons, S., Zhang, F., Rathnachalam, R., Kirkegaard, K., and Colacino, J. M. (2002) *J. Virol.* **76,** 3865–3872
28. Qin, W., Luo, H., Nomura, T., Hayashi, N., Yamashita, T., and Murakami, S. (2002) *J. Biol. Chem.* **277,** 2132–2137
29. Huang, H., Chopra, R., Verdine, G. L., and Harrison, S. C. (1998) *Science* **282,** 1669–1675
30. Doublie, S., Tabor, S., Long, A. M., Richardson, C. C., and Ellenberger, T. (1998) *Nature* **391,** 251–258
31. Cheetham, G. M., and Steitz, T. A. (1999) *Science* **286,** 2305–2309
32. Krausslich, H. G., Holscher, C., Reuer, Q., Harber, J., and Wimmer, E. (1990) *J. Virol.* **64,** 2433–2436
33. Nicklin, M. J., Harris, K. S., Pallai, P. V., and Wimmer, E. (1988) *J. Virol.* **62,** 4586–4593
34. Blair, W. S., Li, X., and Semler, B. L. (1993) *J. Virol.* **67,** 2336–2343
35. Jarvis, T. C., and Kirkegaard, K. (1992) *EMBO J.* **11,** 3135–3145
36. Kirkegaard, K., and Baltimore, D. (1986) *Cell* **47,** 433–443
37. Herold, J., and Andino, R. (2001) *Mol. Cell* **7,** 581–591
38. Barton, D. J., O'Donnell, B. J., and Flanegan, J. B. (2001) *EMBO J.* **20,** 1439–1448
39. Xiang, W., Paul, A. V., and Wimmer, E. (1997) *Semin. Virol.* **8,** 256–273

Structure-Function Relationships of the RNA-dependent RNA Polymerase from Poliovirus (3Dpol): A SURFACE OF THE PRIMARY OLIGOMERIZATION DOMAIN FUNCTIONS IN CAPSID PRECURSOR PROCESSING AND VPg URIDYLYLATION

Harsh B. Pathak, Saikat Kumar B. Ghosh, Allan W. Roberts, Suresh D. Sharma, Joshua D. Yoder, Jamie J. Arnold, David W. Gohara, David J. Barton, Aniko V. Paul and Craig E. Cameron

J. Biol. Chem. 2002, 277:31551-31562.
doi: 10.1074/jbc.M204408200 originally published online June 19, 2002

Access the most updated version of this article at doi: 10.1074/jbc.M204408200

Alerts:
- When this article is cited
- When a correction for this article is posted

Click here to choose from all of JBC's e-mail alerts

This article cites 39 references, 27 of which can be accessed free at
http://www.jbc.org/content/277/35/31551.full.html#ref-list-1